energies

MDPI

Article

Electrical Tree and Partial Discharge Characteristics of Silicone Rubber Under Mechanical Pressure

Jingang Su [1,*], Peng Zhang [1], Zhen Liu [1], Xingwang Huang [1], Xianhai Pang [1], Zeping Zheng [2,*] and Tao Han [2]

[1] State Grid Hebei Electric Power Co., Ltd., Electric Power Science Research Institute, Shijiazhuang 050022, China; dyy_zhangp@he.sgcc.com.cn (P.Z.); dyy_liuz@he.sgcc.com.cn (Z.L.); dyy_huangxw@he.sgcc.com.cn (X.H.); dyy_pangxh@he.sgcc.com.cn (X.P.)

[2] School of Electrical and Information Engineering, Tianjin University, Tianjin 300072, China; hant@tju.edu.cn

* Correspondence: sujingang@tju.edu.cn (J.S.); zzp2024@tju.edu.cn (Z.Z.)

Abstract: Silicone rubber (SIR) is a crucial insulating material in cable accessories, but it is also susceptible to faults. In practical applications, mechanical pressure from bending or shrinking can impact the degradation of SIR, necessitating the study of its electrical tree and partial discharge (PD) characteristics under such pressure. This work presents the construction of a test platform for electrical trees under varying pressures to observe their growth process. A high-frequency current transformer is used to measure PD patterns during tree growth, enabling analysis of the effect of PD on tree initiation and propagation under pressure. The experimental results demonstrate a significant decrease in tree inception probability and increase in PD inception voltage under pressure. The pressure also influences the tree structure and PD during the treeing process, where the longest tree with a branch-like structure appears under 800 kPa. The effect of pressure on electrical tree and PD characteristics can be attributed to changes in free volume, alterations in air pressure within the tree channels, and the affected charge accumulation.

Keywords: silicone rubber; electrical tree; partial discharge; mechanical pressure; cable

Citation: Su, J.; Zhang, P.; Liu, Z.; Huang, X.; Pang, X.; Zheng, Z.; Han, T. Electrical Tree and Partial Discharge Characteristics of Silicone Rubber Under Mechanical Pressure. *Energies* **2024**, *17*, 5645. https://doi.org/10.3390/en17225645

Academic Editor: Pietro Romano

Received: 15 October 2024
Revised: 8 November 2024
Accepted: 11 November 2024
Published: 12 November 2024

1. Introduction

With the advancement of urbanization and industrialization, there is an increasing demand for electricity, highlighting the critical importance of ensuring the safety of electrical transmission [1]. As a crucial component in transmission, maintaining the safe and stable operation of power cables is essential for the security and stability of the power system. The joints of power cables, which consist of multiple layers of solid insulation, represent a vulnerable point in cable insulation. During operations, electrical tree is a typical kind of insulation degradation which leads to failure [2,3].

Electrical tree is a pre-breakdown phenomenon that occurs within insulating materials and is one of the main problems causing faults in high-voltage cables and cable accessories. The breakdown of solid dielectrics can be attributed to a series of local pre-breakdown channels, which are generated due to the existence of defects in the insulation structure. Around the defective parts of these dielectric structures, channels resembling the branches of a tree will be formed, which are called electrical trees [4]. Electrical trees form in solid insulation as a result of PD (partial discharge), which are widely present in various insulating materials, and are one of the important reasons for the degradation of cable insulation. Electrical trees can exist in materials such as epoxy resin, crosslinked polyethylene (XLPE), silicone rubber (SIR), and polypropylene (PP) [5,6]. The formation of electrical tree channels usually leads to breakdown of the insulation material, resulting in failure [7,8].

SIR is a crucial insulating material used in 10–35 kV cold shrink joints and can be made into the cold shrink joints which can be fixed onto a cable joint, relying only on its own elasticity without heating. In operational conditions with local distorted electric fields, it may also lead to the inception of electrical trees in SIR. Therefore, it is necessary to simulate

the environment in the cold shrink tube and conduct an electrical tree test. Various factors can influence the inception and growth of electrical trees during the use of SIR. The tree channel in SIR appears to be white in color under natural light, distinguishing it from other insulating materials, and its shape changes with temperature [9]. As the temperature increases from 30 to 90 °C, the morphology of electrical trees gradually transitions from a branch structure to a bush structure [9]. Additionally, the temperature gradient present in SIR causes variations in tree initiation voltage, length, and structure [10]. One study found that with increased tensile mechanical stress, the tree initial voltage decreased from 15.30 kV to 14.33 kV, and the electrical tree tended to grow in the direction of stress application [11]. Moreover, high current-generated magnetic fields have a positive effect on promoting the growth of electrical trees, with the effect threshold at 400 mT [12]. To inhibit electrical treeing in SIR, nanocomposites have been introduced into dielectric applications. Due to their substantial specific surface area and two-dimensional structure, graphene nanosheets effectively suppress the initiation and growth of electrical trees in SIR [13,14]. Additionally, non-metallic oxide silicon dioxide has been demonstrated to inhibit the formation of electrical trees in SIR at appropriate additive concentrations [15,16]. Furthermore, materials such as ferric oxide and aluminum oxide have been investigated for their potential to be mixed into SIR to hinder electrical treeing [17,18]. Moreover, some researchers have analyzed the generation mechanism and growth process of electrical tree channels on the XLPE-SIR interface. Their findings indicate that roughness and interface stress are critical factors influencing electrical treeing [19–21].

PD has been a focal point for numerous researchers as it is the primary driving force for the development of electrical trees. Synchronous analysis of PD during electrical tree growth is crucial in uncovering the dynamic characteristics of electrical trees [22]. In the course of electrical tree growth, there is both PD at the needle tip and PD caused by internal space charge accumulation, with some channels forming conductive streamers that propagate through the branches to facilitate charge transport [23,24]. Researchers have also observed that the conductivity of the tree channel itself plays a key role in shaping the tree, with pine branch channels exhibiting higher conductivity and branch channels showing lower conductivity in XLPE [25]. The phenomenon of PD has also been utilized to characterize the developmental state of electrical trees [26]. The correlation dimension and maximum Lyapunov index of PD sequences are associated with tree growth, rather than random processes [27]. Additionally, a low-frequency power ratio and equivalent bandwidth parameters prove to be more sensitive indicators for tracking tree progression and align with tree length [26].

However, the SIR cable joint material may suffer from extrusion deformation under mechanical pressure, such as self-stress or external bending, potentially altering the growth characteristics of electrical trees and causing a change in PD [28–30]. This pressure will influence both the PD and electrical trees. However, there is still a lack of research on the relationships among the growth of electrical trees, pressure, and PD in SIR, and the tree inception and growth characteristics need to be illustrated, considering PD as the promoting factor.

A testing platform for SIR electrical trees under varying levels of mechanical pressure was established in this work to determine the relationships between the mechanical pressure, electrical tree, and PD. The tree inception voltage, tree structure, and their growth were recorded. PD signals were also detected. Through the analysis of electrical trees and PD signals, the free volume was found to be the reason for increased tree inception voltage. The changed channel width, gas pressure, and charge accumulation inside the channels were the key reasons for different tree processes under different pressures.

2. Experiment Platform

As shown in Figure 1, the electrical tree test platform mainly comprises a power supply system, a microscope recording system, and a PD detection system. High-voltage AC power is provided using a voltage of 50 Hz and 220 V through the transformer (CHINT, TDGC 2–3). A high-voltage resistor is utilized to protect the samples. During the application of voltage, the sample is immersed in silicone oil to minimize the impact of discharge out of the sample. Before applying voltage, a cold light source is turned on and the microscope is adjusted such that the electrical tree shape captured with the microscope can be seen and recorded on the computer. A high-frequency current transformer (HFCT) with a bandwidth of 100 kHz to 50 MHz is applied to the ground cable for monitoring PD while the electrical tree is developing. The PD detection system processes the data and generates the phase-resolved partial discharge (PRPD) diagram, from which the information regarding the amplitude and phase distribution of the PD can be extracted.

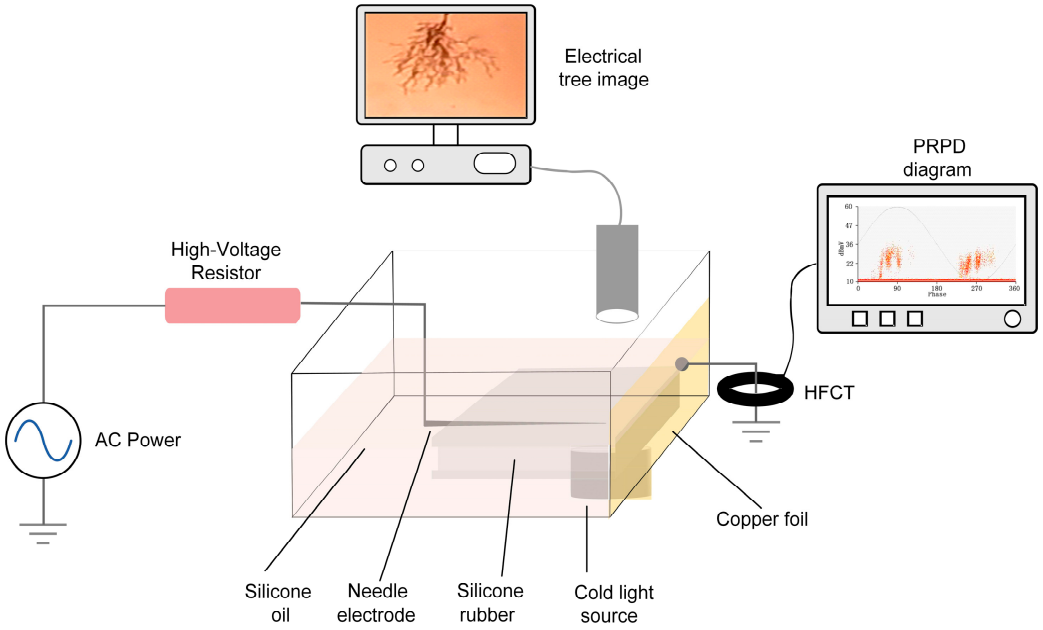

Figure 1. Experiment platform for tree and PD test.

3. Sample Preparation

The high-voltage electrode is constructed with a needle featuring a 30° cone angle, a 2 μm radius of curvature, and a 30 μm diameter. The ground electrode is a copper foil attached to the bottom to ensure grounding without impacting pressure application. The distance between the needle tip and the ground electrode is set to be 2 mm [31,32].

The electric field around the needle tip can be obtained using the Mason formula, as follows:

$$E = \frac{2U}{R\ln(1+\frac{4d}{R})}, \quad (1)$$

where E is the electric field intensity, U is the amplitude of applied voltage, R is the radius of curvature of the tip, and d is the distance from the tip to the ground electrode.

Existing research has shown that when the pressure at the interface between cable accessories and the main insulation is within the range of 100 kPa to 250 kPa, the requirements for electrical insulation can be met [29]. Therefore, the pressure range in this work was chosen to be 0 to 800 kPa, in order to simulate the possible pressure in installation and operation.

During the experiment, pressure was applied through the structure shown in Figure 2. The set stress was obtained by adjusting the screws on the sample. In this work, the deformation of SIR during the pressurization process was measured, and the results are shown in Table 1.

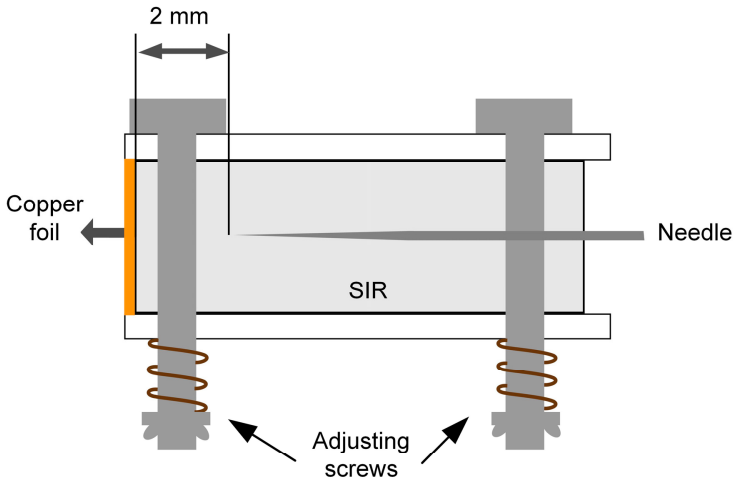

Figure 2. Structure of sample for test.

Table 1. Corresponding relationship between SIR deformation and pressure.

Pressure (kPa)	Thickness (mm)	Thickness Deformation (%)
0	5.73	0
200	5.42	−5.41
400	5.18	−9.60
600	5.11	−10.82
800	5.03	−12.22

4. Results

4.1. Electrical Tree Inception

Figure 3 illustrates the tree inception probability at 8.5 kV voltage after 5 min; 20 samples were tested under each pressure. The tree was considered to be triggered if a visible branch longer than 20 μm was observed near the needle tip. At 0 kPa, the tree inception probability is 90%, while at 800 kPa, it decreases to only 60%. A sharp decrease occurs when the pressure is increased to 400 kPa. It is evident that the pressure on SIR has a negative effect on tree inception at the same voltage.

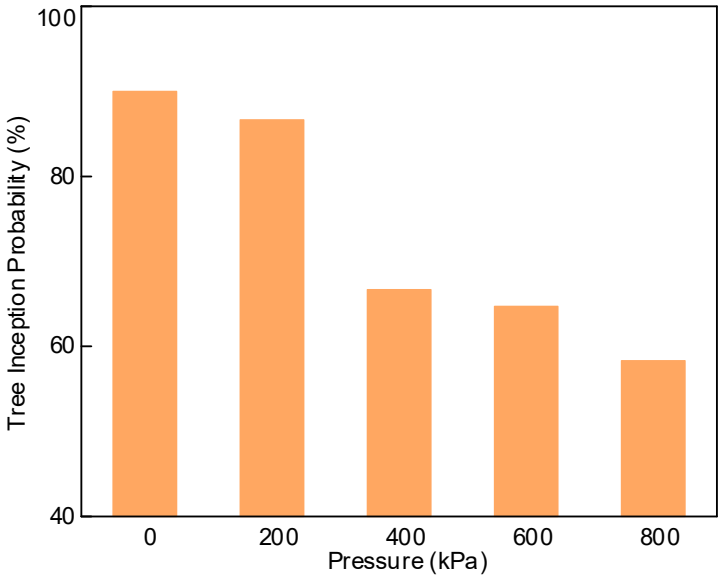

Figure 3. Electrical tree inception probability under each pressure.

4.2. Electrical Tree Morphology

In the experiment, the growth time of the electrical trees was set at 60 min. The morphology of the electrical trees under varying pressures exhibits significant variation, with bush-like and branch-like structures being the predominant morphologies. The typical bush-like electrical trees are depicted in Figure 4a, while the typical branch-like trees are illustrated in Figure 4c. It is observed that as pressure increases, the proportion of bush-like trees gradually decreases, with no discernible bush-like branches present under a pressure of 800 kPa. As shown in Figure 4a, numerous interleaved tiny tree channels are evident within the bush-like trees, accompanied by a large dark area at their center. This dark area indicates that a substantial number of channels were shielded from light when photographed using back light. Under a pressure of 400 kPa, it is noted that while the width of the channel remains similar to that of bush-like trees, there is a significant reduction in their number, and they begin to adopt a shape more closely resembling branch-like trees. Upon reaching a pressure level of 800 kPa, distinct main channels become apparent within the electrical tree region, generally numbering between two and five, and exhibiting larger width and longer channel lengths.

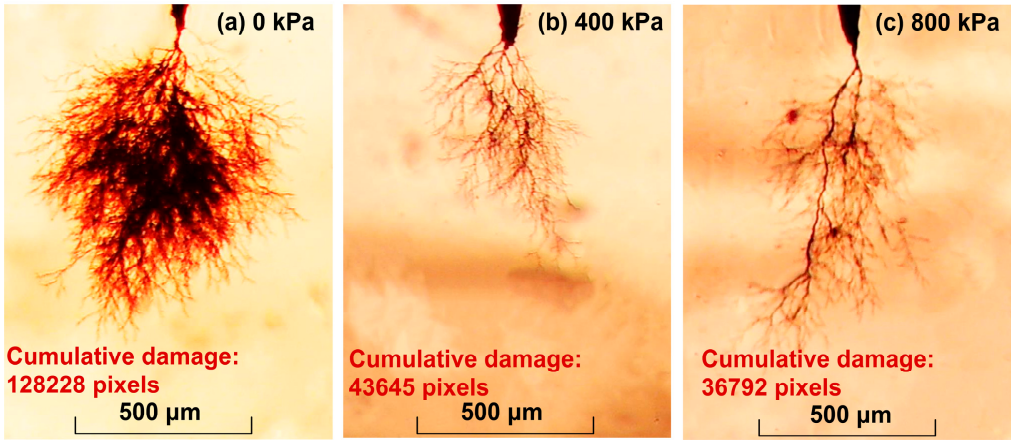

Figure 4. Morphology of electrical trees.

Cumulative damage can be clearly understood as the number of pixels occupied by the area where the degradation appears. When it is used in tree analysis, it shows the damaged area of insulation created by the electrical trees. The cumulative damage of the electrical trees can be calculated by removing color and binarizing the original image. Figure 4 illustrates the cumulative damage of electrical trees. It is evident that as the pressure increases, there is a decreasing trend in cumulative damage, which changes from 128,228 to 36,792 pixels.

4.3. Electrical Tree Growth

To comprehend the variations in tree length during their growth, 10 samples were tested under each pressure. The length of each typical tree under every level of pressure was calculated as the growth length of electrical trees at the treeing time. To clearly illustrate the growth trend of electrical trees under varying pressures and streamline the data analysis in this study, we focused on analyzing the growth process of electrical trees at 0, 400, and 800 kPa. It was observed that the growth trend at 200 and 600 kPa exhibited similarities to those at 0 and 800 kPa, respectively.

Figure 5 illustrates the growth trend of three typical electrical trees. The presence of pressure results in noticeable variations in tree length and growth characteristics. Within the initial 5 min, the length of electrical trees under each level of pressure experiences rapid growth to over 50% of total length, with the fastest growth rate observed at 0 kPa and the slowest at 400 kPa. Subsequently, between 5 and 15 min, electrical trees at 0 and 400 kPa remain stagnant for an extended period, while the tree under 800 kPa continues to

grow slowly. From this point until 60 min, electrical trees at 0 kPa only exhibit a growth of approximately 50 µm, closely associated with their morphology at this voltage. The bush-like electrical trees primarily demonstrate the continuous generation of tiny branches during the growth process, leading to a deceleration in their length expansion. The final morphology of trees at both 400 and 800 kPa differs significantly from bush-like; they show a branch structure with main channels visible under high pressures. Although both types of electrical trees continue to elongate between 15 and 60 min, their growth rate is slower than the initial stage. Notably, in more than 80% of the samples, the tree length is the longest under 800 kPa at 60 min.

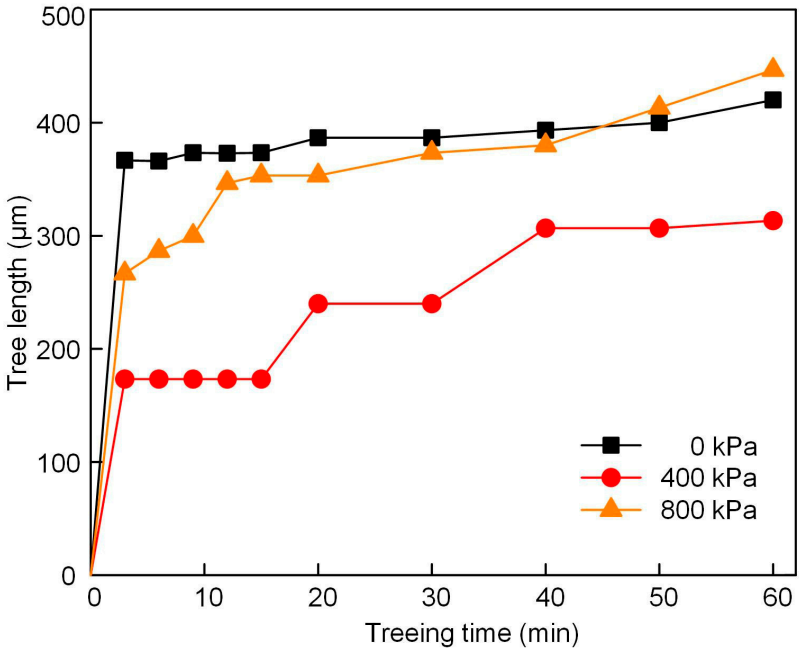

Figure 5. Electrical tree growth under different levels of pressure.

4.4. Partial Discharge in Tree Inception

A PD will occur before the tree is observed during the tree initiation. To confirm the effect of pressure on this process, the partial discharge inception voltage (PDIV) of the pin–plate electrode was tested under different pressure conditions. During testing, a gradient increasing voltage with 0.2 kV/30 s was applied, and the PD testing method depicted in Figure 1 was utilized to determine the PDIV. The results, as illustrated in Figure 6, indicate an increase in average PDIV from 8.5 kV to approximately 9 kV with increasing pressure. Furthermore, it is observed that the dispersion of PDIV decreases with rising mechanical pressure, suggesting a significant inhibition effect on the inception voltage of PD in the needle electrode due to increased pressure.

4.5. Partial Discharge in Tree Growth

While measuring and recording the growth of electrical trees, the PD characteristics were also observed. Figure 7 illustrates the trend of changes in PD intensity during electrical tree growth, with the maximum discharge amplitude recorded for each stage. Additionally, Figure 8 displays the PRPD spectrum at different pressures, providing direct insight into discharge intensity and phase distribution information. It is evident from the figures that morphological features of PRPD vary with the growth of electrical trees. With different pressures, they show consistency only in the initial stage and significant differences thereafter.

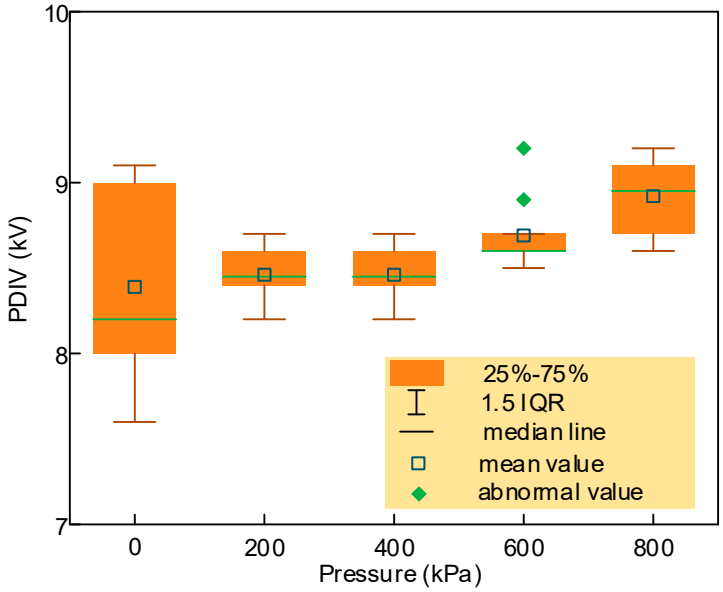

Figure 6. PDIV under different levels of pressure.

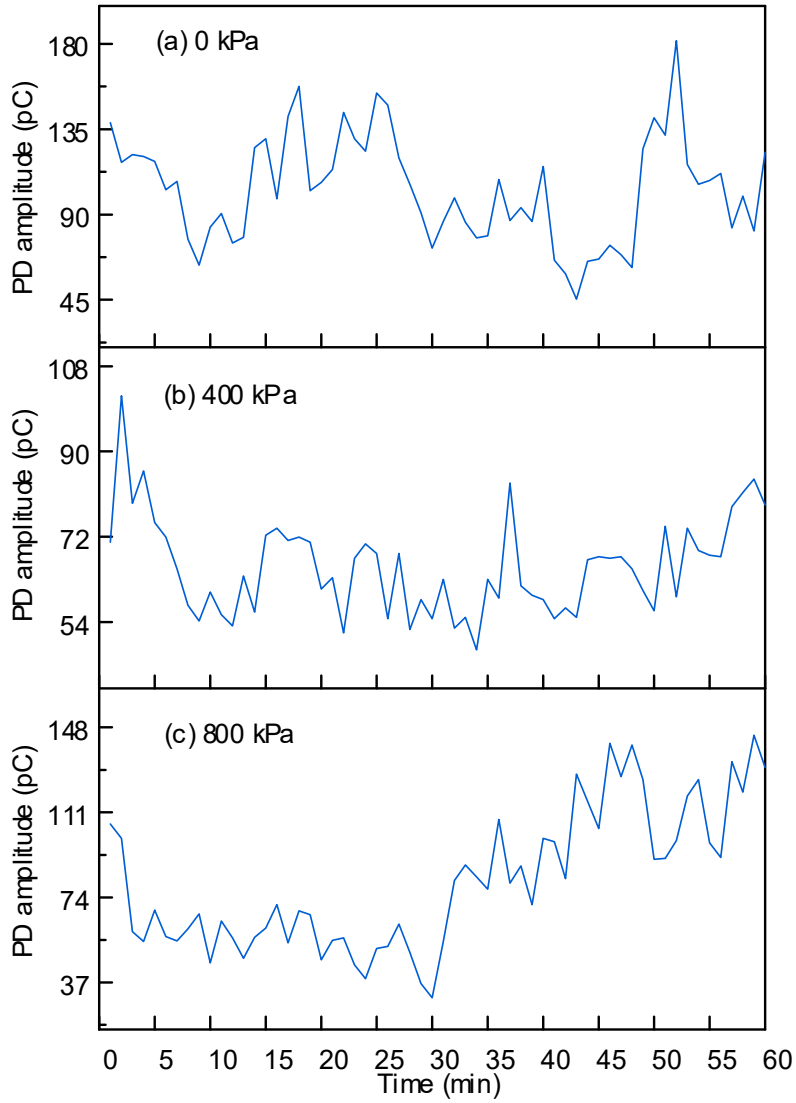

Figure 7. Changes in the PD amplitude during treeing time.

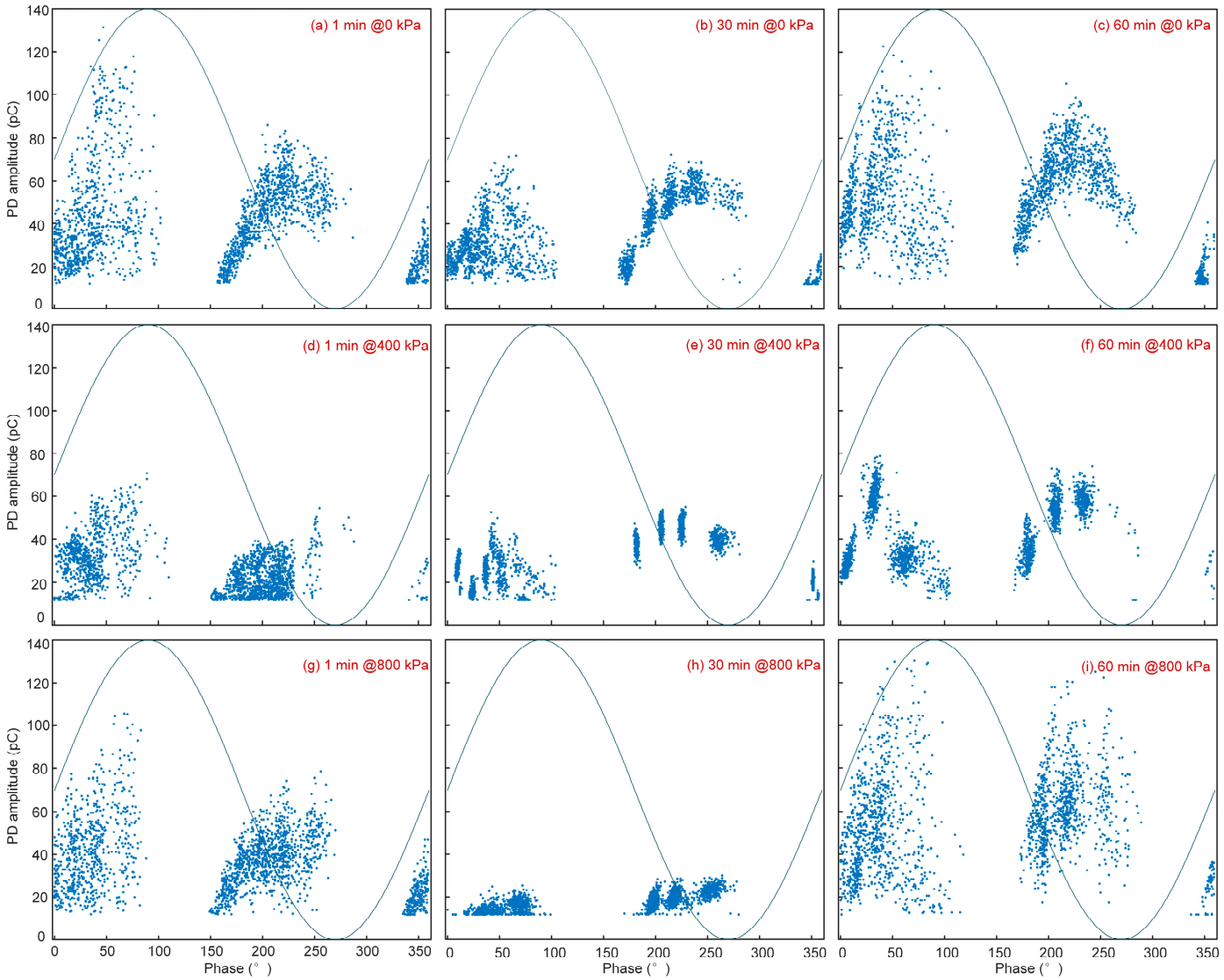

Figure 8. PRPD under different pressures.

As depicted in Figure 7a, three peak periods of PD intensity are observed in the sample at 0 kPa, specifically at 0–7 min, 15–25 min, and 50–55 min. During the initial stage, the rate of attenuation in discharge amplitude is notably slower compared to other pressures. Throughout the entire discharge process, there is consistency in the shape of PRPD, with variations only in discharge intensity, as shown in Figure 8a–c. Discharges are concentrated within the first and third quadrants, while at the beginning and end of treeing time, discharge intensity in the positive half-cycle significantly exceeds that in the negative half-cycle. In Figure 8b, a decrease in PD intensity is evident primarily through attenuation in positive half-cycle discharge amplitude. However, there is no significant change observed in its phase distribution.

As depicted in Figure 7b, the initial PD intensity under 400 kPa is notably lower than that at 0 kPa, and the amplitude is below 100 pC throughout the growth of electrical trees after 2 min. At 1 min, the PRPD morphology is similar to that at 0 kPa. However, after 10 min, there is a change in PRPD morphology, as illustrated in Figure 8e, wherein positive and negative half-cycle discharge amplitudes become similar, yet the discharge becomes concentrated in four narrow phase windows within the third quadrant. The phase distribution of PD ceases to be continuous, and this morphological feature persists until 60 min. This observation indicates that pressure significantly inhibits PD, resulting in amplitude and phase differences.

When the pressure reaches 800 kPa, the PD intensity exhibits three distinct stages. As depicted in Figure 7c, the initial stage demonstrates a relatively high intensity, which then decays to less than 50% of its initial level within approximately 2 min. This low-intensity discharge persists for up to 30 min, followed by a subsequent increase in discharge intensity, consistently displaying strong PD until 60 min. However, between 2 and 30 min, PRPD manifests as two clusters of discharges with low amplitudes, as shown in Figure 8h. In the third stage, there is an observable change in PRPD morphology alongside an increase in discharge amplitude, as illustrated in Figure 8i.

The T-F Map method is a well-established technique for characterizing the features of PD in the time–frequency domain, and it can effectively differentiate the variations in PD distribution within this domain [33]. Following the acquisition of PD signal waveforms in the time domain, T-F map calculations are performed at each treeing time. The results indicate that the equivalent time distribution of PD signals remains consistent across different time periods, while there are noticeable variations in frequency distribution with changes in pressure. Specifically, analysis was conducted on T-F Map data under different pressures at 1 min, as depicted in Figure 9. It is evident from the figure that as the pressure increases gradually, the frequency center decreases from 19.3 MHz under 0 kPa to 17.8 MHz under 800 kPa. This phenomenon exists throughout the whole treeing process.

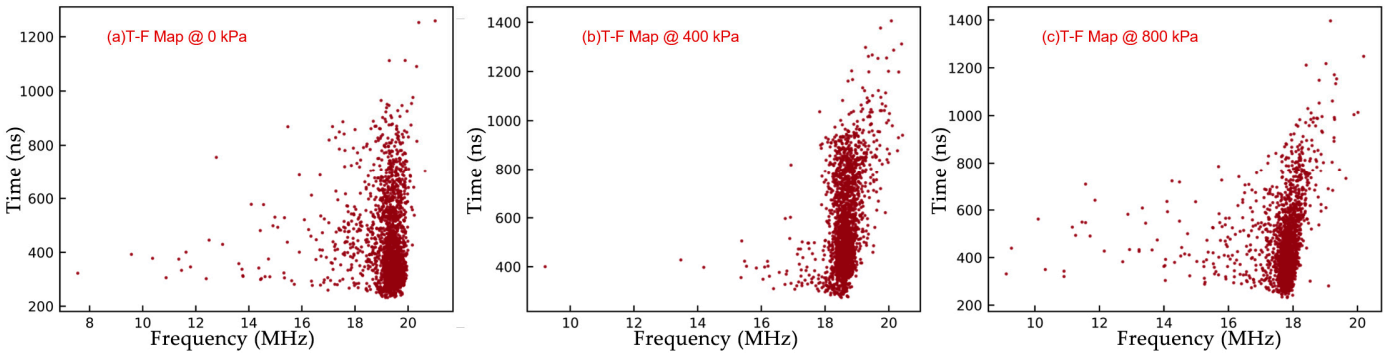

Figure 9. T-F Map under different pressures at 1 min.

5. Discussion

5.1. Effect of Pressure on Tree Inception

The first factor that affects the tree inception process is the change in free volume of SIR for electrical trees grown under different pressures [34]. The term "free volume" refers to the unoccupied space between molecular chains, and it can also be described as the distance between molecular chains. After the insertion of the needle electrode, free electrons will accelerate and gain energy in this region due to the presence of the electric field. This concept is closely related to the electrical tree resistance of insulation materials. However, the size of the free volume will be altered with the bulk deformation. As shown in Table 1, the free volume decreases with the shrinking of the sample under the different mechanical pressures. The pressure will also make the molecular chain shift, filling the free volume near the needle tip. The most important process during tree inception is the acceleration of electrons and their collisions with molecular chains, resulting in a small region of low density. While under pressure, the formation of this region will be delayed by the constant pressure, which will cause the free volume between molecules to shrink in some directions. As a result, the energy obtained by electrons under the influence of the electric field will be diminished, weakening insulation damage and leading to a lower tree inception probability.

When a low-density area forms and reaches a sufficient size, PD will occur within this region. The heat, light, and gas produced by the PD will result in further damage to the SIR material. Subsequently, observable initial tree channels will form in the damaged area due to PD erosion. However, under different pressures, the occurrence of PD at this initial stage will be altered by the size of the low-density region. Specifically, the formation

of the induced PD within the low-density region will proceed more slowly under greater pressure. This influence leads to a gradual increase in PDIV as pressure rises and a decrease in PDIV dispersion.

5.2. Effect of Pressure on Tree Growth

During the development of electrical trees, significant variation in their morphology and PD intensity is observed. These differences are closely associated with the influence of distinct pressures, a topic that will be further explored in this section.

PD is considered to be the primary driving force for the generation of new branches and the alteration in the length of electrical trees during their growth. These factors influence the promotion of electrical trees involved in the generation of heat, light, and accelerated charges during PD. When the pressure is applied, it directly influences the PD process, thereby impacting the growth process of electrical trees.

PD occurs both at the needle tip and in part of the tree channels. The presence of the needle tip causes significant electric field distortion at the root of the branch, facilitating initiation of discharge into a gas environment. In the absence of pressure, a substantial amount of gas is present in the gradually widening branch channel, forming a conductor-silicone rubber-gas contact interface at the tip position, which will cause an intense PD and accelerate tree growth, as shown in Figures 7 and 8. However, under the influence of pressure, the electrical tree at the tip of the needle experiences a reduction in width due to pressure, particularly at 800 kPa (as depicted in Figure 7). It is evident that both the intensity and phase distribution of PD decrease significantly, especially between 5 and 30 min. Furthermore, the accumulation of charge caused by the trap distributed in the tree channel will also induce a local high space charge field, leading to discharge and triggering new tree channels. When there is no pressure, this kind of PD will occur randomly and produce a large number of tiny channels. However, when subjected to pressure, the tree channels experience continuous compression, leading to a blockage in the charge migration process within the air gap. This ultimately results in the failure to randomly form local high electric fields in the existing channels. Consequently, there is a decrease in the number of newly generated channels as pressure increases, causing the morphology of the trees to transition gradually from a bush-like to a branch-like structure.

During the development of electrical trees, the gas produced by PD accumulates in the branch channel, and the air pressure within the channel fluctuates with the level of discharge. Simultaneously, this gas pressure also impacts the inception voltage and intensity of PD. According to the literature, the PDIV increases with higher air pressure [35]. The SIR material exhibits high elasticity under normal pressure and demonstrates good resilience. As the air pressure within the channel rises, the surrounding SIR material will expand accordingly. The expansion process ceases when the stress from silicone rubber deformation balances with that generated by internal gas pressure. However, when subjected to high external mechanical pressure, the expansion of material caused by the gas is diminished. This results in a significant increase in gas pressure, thereby elevating the PDIV within the channel. Consequently, this effect leads to changes in the PRPD, especially in trees with a short length and fewer channels.

It is important to note that when the pressure reaches 800 kPa, there are significant main channels with a notably greater width compared to other channels. This phenomenon can be attributed to the intense erosion resulting from continuous discharge within a single channel. Under very high external pressure, fewer initial branches are formed, leading to more concentrated PD at the needle tip and within the channel. Following prolonged erosion (30 min in the sample depicted in Figure 7c), this channel undergoes noticeable widening, resulting in reduced inhibition of mechanical pressure on PD. As a result, more intense PD occurs and accelerates the growth of these tree channels, forming branch-like trees, as depicted in Figure 4c.

6. Conclusions

In this work, the characteristics of electrical tree and PD in SIR under pressure were investigated. The key findings are as follows:

(1) With mechanism pressure increasing from 0 to 800 kPa, the tree inception probability decreases from 90% to 60%, and the average PDIV increases from 8.5 to 9 kV. This provides evidence for the inhibition effect of pressure on tree inception.
(2) At 60 min, the morphology of electrical trees undergoes a gradual transition from a bush-like structure to a branch-like structure as pressure increases, ultimately resulting in all trees having a branch-like structure under 800 kPa. The slowest growth rate occurs at 400 kPa.
(3) The lowest PD amplitude appears at 400 kPa, consistent with the growth rate of electrical trees, and there is a decrease in the frequency center of PD signals with the T-F map analysis.
(4) The pressure restricts the inception of PD and the formation of initial trees by influencing the free volume. It also alters the morphology of electrical trees through its impact on internal gas pressure and charge accumulation.

Author Contributions: Methodology, J.S. and P.Z.; software, J.S., Z.L. and X.P.; validation, P.Z.; formal analysis, P.Z. and X.P.; investigation, J.S., Z.L. and X.P.; resources, P.Z. and X.H.; data curation, P.Z. and X.H.; writing—original draft preparation, Z.Z., J.S. and P.Z.; writing—review and editing, J.S. and X.H.; funding acquisition, J.S. and T.H. All authors have read and agreed to the published version of the manuscript.

Funding: This research was funded by the Science and Technology Project of the State Grid Corporation of China, grant number kj2023-046.

Institutional Review Board Statement: Not applicable.

Informed Consent Statement: Not applicable.

Data Availability Statement: Data available upon request from the authors.

Conflicts of Interest: Authors Jingang Su, Peng Zhang, Zhen Liu, Xingwang Huang and Xianhai Pang were employed by the State Grid Hebei Electric Power Co., Ltd. The remaining authors declare that the research was conducted in the absence of any commercial or financial relationships that could be construed as a potential conflict of interest.

References

1. Arnob, S.S.; Arefin, A.I.M.S.; Saber, A.Y.; Mamun, K.A. Energy demand forecasting and optimizing electric systems for developing countries. *IEEE Access* **2023**, *11*, 39751–39775. [CrossRef]
2. Zhou, Y.; He, J.L.; Hu, J.; Huang, X.Y.; Jiang, P.K. Evaluation of polypropylene/polyolefin elastomer blends for potential recyclable HVDC cable insulation applications. *IEEE Trans. Dielectr. Electr. Insul.* **2015**, *22*, 673–681. [CrossRef]
3. Källstrand, B.; Borg, D.; Walfridsson, L.; Johansson, K.; Doiron, C.; Fälth, F. DC Field Distribution around an HVDC Cable Termination. In Proceedings of the IEEE Conference on Electrical Insulation Dielectric Phenomena (CEIDP), Ann Arbor, MI, USA, 18–21 October 2015.
4. Zhang, Z.; Zheng, S.; Zhao, Y.; Liu, D.; Wu, S. Effects of Tip Radius of Curvature on Electrical Tree Growth and Partial Discharge Characteristics of XLPE. In Proceedings of the 2021 IEEE 2nd China International Youth Conference on Electrical Engineering (CIYCEE), Chengdu, China, 15–17 December 2021.
5. Yang, Z.; Tong, B.; Wang, H.; Zhu, P.; Rao, H.; Li, Z. Enhanced electrical tree resistance of polypropylene cable insulation by introducing β-crystals. *Energies* **2024**, *17*, 4610. [CrossRef]
6. Liu, H.; Wu, X.; Guo, Z.; Dong, P.; Ge, Q.; Wei, L.; Sun, Z. Electrical tree characteristics of bisphenol epoxy resin/maleopimaric anhydride curing system. *Polymers* **2022**, *14*, 3867. [CrossRef] [PubMed]
7. Danikas, M.G.; Tanaka, T. Nanocomposites-a review of electrical treeing and breakdown. *IEEE Electr. Insul. Mag.* **2009**, *25*, 19–25. [CrossRef]
8. Dissado, L.A. Understanding electrical trees in solids: From experiment to theory. *IEEE Trans. Dielectr. Electr. Insul.* **2002**, *9*, 483–497. [CrossRef]
9. Du, B.X.; Ma, Z.L.; Gao, Y.; Han, T. Effect of ambient temperature on electrical treeing characteristics in silicone rubber. *IEEE Trans. Dielectr. Electr. Insul.* **2011**, *18*, 401–407. [CrossRef]

10. Zhang, Y.X.; Zhang, L.; Zhou, Y.X.; Chen, M.; Zhou, Z.L.; Liu, J. DC electrical tree initiation in silicone rubber under temperature gradient. *IEEE Trans. Dielectr. Electr. Insul.* **2018**, *25*, 1142–1150. [CrossRef]
11. Weisun, J.X.; Wang, S.P.; Xu, M. Effect of Large Mechanical Stress on Electrical Tree Characteristics of Silicone Rubber. In Proceedings of the 2021 IEEE International Conference on the Properties and Applications of Dielectric Materials (ICPADM), Johor Bahru, Malaysia, 12–14 July 2021.
12. Han, T.; Du, B.X.; Li, J.; Le Ma, Z.; Guo, Y.G.; Zhang, X.Q. Effect of Magnetic Field on Tree Characteristics in Silicone Rubber. In Proceedings of the 2015 IEEE International Conference on Applied Superconductivity and Electromagnetic Devices (ASEMD), Shanghai, China, 20–23 November 2015.
13. Du, B.; Liu, H.; Li, F.; Kong, X.; Du, H.; Liang, H. Effects of gradient magnetic field on electrical tree growth of SIR/graphene nanocomposites. *IEEE Trans. Dielectr. Electr. Insul.* **2023**, *30*, 1966–1973. [CrossRef]
14. Li, Y.; Du, B.; Li, J.; Li, Z.; Han, T.; Ran, Z. Electrical Tree Characteristics in Graphene/SIR Nanocomposites under Temperature Gradient. In Proceedings of the 2021 International Conference on Electrical Materials and Power Equipment (ICEMPE), Chongqing, China, 11–15 April 2021.
15. Ibrahim, M.E.; Abd-Elhady, A.M.; Elmasry, E.S.; Izzularab, M.A. Evaluation of Electrical Treeing and Dielectric Spectroscopy of Silicone Rubber Nanocomposites under Thermal Ageing. In Proceedings of the 2021 22nd International Middle East Power Systems Conference (MEPCON), Assiut, Egypt, 14–16 December 2021.
16. Han, T.; Du, B.X.; Yu, Y.; Zhang, X.Q. Effect of cryogenic temperature on tree characteristics in silicone rubber/SiO_2 nanocomposites under repetitive pulse voltage. *IEEE Trans. Appl. Supercond.* **2016**, *26*, 1–4. [CrossRef]
17. Wang, M.; Yin, X.; Liu, Y.; Du, B.; Xue, C. Electrical treeing of sir and SIR/Fe_3O_4 nanocomposites in high magnetic field. *IEEE Access* **2023**, *11*, 52614–52621.
18. Hafiz, M.; Fairus, M.; Mansor, N.S.; Kamarol, M.; Mariatti, M. Investigation of Electrical Treeing Structures in SIR/Alumina Nanocomposites. In Proceedings of the IEEE Conference on Energy Conversion (CENCON), Johor Bahru, Malaysia, 19–20 October 2015.
19. Zhu, G.Y.; Liu, Z.G.; Wang, W.G.; Zhou, K.; Lu, L.; Shen, Q.; Pan, S.K.; Ma, S.Y.; Shao, Y. Investigation of interface discharge characteristics for cable accessories after moisture penetration into the XLPE–SIR interface. *IEEE Trans. Dielectr. Electr. Insul.* **2023**, *30*, 2285–2294. [CrossRef]
20. Li, Q.; Zhang, Y.; Tang, X.; Li, Z. Study on Partial Discharge Characteristics During Electrical Tree Growth at XLPE-SIR Interface. In Proceedings of the International Conference on Power System Technology (POWERCON), Haikou, China, 8–9 December 2021.
21. Su, Y.; Liu, Y.; Lian, R.; Gao, X.; Zhong, L. Effect of Surface Smoothness on Electrical Tree Characteristics at XLPE-SIR Interface. In Proceedings of the International Conference on Electrical Materials and Power Equipment (ICEMPE), Guangzhou, China, 7–10 April 2019.
22. Yang, Z.; Gao, Y.; Deng, J.; Lv, L. Partial discharge characteristics and growth stage recognition of electrical tree in XLPE insulation. *IEEE Access* **2023**, *11*, 145527–145535. [CrossRef]
23. Lv, Z.; Rowl, S.M.; Chen, S.; Zheng, H.; Wu, K. Modelling of partial discharge characteristics in electrical tree channels: Estimating the PD inception and extinction voltages. *IEEE Trans. Dielectr. Electr. Insul.* **2018**, *25*, 1999–2010. [CrossRef]
24. Zhu, X.; Wu, J.; Wang, Y.; Yin, Y. Characteristics of partial discharge and AC electrical tree in XLPE and MgO/XLPE nanocomposites. *IEEE Trans. Dielectr. Electr. Insul.* **2020**, *27*, 450–458. [CrossRef]
25. Chen, X.; Xu, Y.; Cao, X.; Gubanski, S.M. On the conducting and non-conducting electrical trees in XLPE cable insulation specimens. *IEEE Trans. Dielectr. Electr. Insul.* **2016**, *23*, 95–103. [CrossRef]
26. Abdel-Galil, T.K.; Sharkawy, R.M.; Salama, M.M.A.; Bartnikas, R. Partial discharge pattern classification using the fuzzy decision tree approach. *IEEE Trans. Dielectr. Electr. Insul.* **2005**, *54*, 2258–2263. [CrossRef]
27. Chen, X.; Xu, Y.; Cao, X. Nonlinear time series analysis of partial discharges in electrical trees of XLPE cable insulation samples. *IEEE Trans. Dielectr. Electr. Insul.* **2014**, *21*, 1455–1461. [CrossRef]
28. Borthakur, D.P.; Verma, A.R. Thermo-Mechanical and Electrical Stress Analyses of HVDC Cable Joint with Load Cycle. In Proceedings of the 2024 IEEE International Conference on High Voltage Engineering and Applications (ICHVE), Berlin, Germany, 18–22 August 2024.
29. Hamdan, M.A.; Pilgrim, J.A.; Lewin, P.L. The Temperature Dependence of Insulation Mechanical Properties and its Effect on Interface Pressure in Cable Joints. In Proceedings of the 2018 IEEE 2nd International Conference on Dielectrics (ICD), Budapest, Hungary, 1–5 July 2018.
30. Song, M.; Jia, Z. Calculation and Simulation of Mechanical Pressure of XLPE-SR Surface in Cable Joints. In Proceedings of the 2018 12th International Conference on the Properties and Applications of Dielectric Materials (ICPADM), Xi'an, China, 20–24 May 2018.
31. Sahoo, R.; Karmakar, S. Impact of accelerated thermal aging on electrical tree structure and physicochemical characteristics of XLPE insulation. *IEEE Trans. Dielectr. Electr. Insul.* **2023**, *31*, 429–438. [CrossRef]
32. Yabuuchi, W.; Wada, A.; Sasaki, S.; Kawai, Y.; Hyeon-Gu, J.; Fujii, M.; Ihori, H. Electric Field Strength and Tree Propagation Speed for Electrical Treeing in Silicone Gel. In Proceedings of the 2020 International Symposium on Electrical Insulating Materials (ISEIM), Tokyo, Japan, 13–17 September 2020.
33. Cavallini, A.; Montanari, G.C.; Contin, A.; Pulletti, F. A new approach to the diagnosis of solid insulation systems based on PD signal inference. *IEEE Electr. Insul. Mag.* **2003**, *19*, 23–30. [CrossRef]

34. Shimizu, N.; Tanaka, H. Effect of liquid impregnation on electrical tree initiation in XLPE. *IEEE Trans. Dielectr. Electr. Insul.* **2001**, *8*, 239–243. [CrossRef]
35. Lusuardi, L.; Rumi, A.; Cavallini, A.; Barater, D.; Nuzzo, S. Partial discharge phenomena in electrical machines for the more electrical aircraft. Part II: Impact of reduced pressures and wide bandgap devices. *IEEE Access* **2021**, *9*, 27485–27495. [CrossRef]